Clim Dyn (2010) 35:887–905
DOI 10.1007/s00382-009-0633-5

The transition from the present-day climate to a modern Snowball Earth

Aiko Voigt · Jochem Marotzke

Received: 12 February 2009 / Accepted: 7 July 2009 / Published online: 29 July 2009
© The Author(s) 2009. This article is published with open access at Springerlink.com

Abstract We use the coupled atmosphere–ocean general circulation model ECHAM5/MPI-OM to investigate the transition from the present-day climate to a modern Snowball Earth, defined as the Earth in modern geography with complete sea-ice cover. Starting from the present-day climate and applying an abrupt decrease of total solar irradiance (TSI) we find that the critical TSI marking the Snowball Earth bifurcation point is between 91 and 94% of the present-day TSI. The Snowball Earth bifurcation point as well as the transition times are well reproduced by a zero-dimensional energy balance model of the mean ocean potential temperature. During the transition, the asymmetric distribution of continents between the Northern and Southern Hemisphere causes heat transports toward the more water-covered Southern Hemisphere. This is accompanied by an intensification of the southern Hadley cell and the wind-driven subtropical ocean cells by a factor of 4. If we set back TSI to 100% shortly before the transition to a modern Snowball Earth is completed, a narrow band of open equatorial water is sufficient for rapid melting. This implies that for 100% TSI the point of unstoppable glaciation separating partial from complete sea-ice cover is much closer to complete sea-ice cover than in classical energy balance models. Stable states can have no greater than 56.6% sea-ice cover implying that ECHAM5/MPI-OM does not exhibit stable states with near-complete sea-ice cover but open equatorial waters.

Keywords Snowball Earth · General circulation model · Energy balance model · Bifurcation point · Transition times · Clouds · Water vapor · Heat transports · Point of unstoppable glaciation

A. Voigt (✉)
International Max Planck Research School on Earth System Modelling, Bundesstrasse 53, 20146 Hamburg, Germany
e-mail: aiko.voigt@zmaw.de

A. Voigt · J. Marotzke
Max Planck Institute for Meteorology, Bundesstrasse 53, 20146 Hamburg, Germany
e-mail: jochem.marotzke@zmaw.de

1 Introduction

Earth's climate can exhibit at least two entirely different modes as suggested by climate models (Budyko 1969; Sellers 1969; Poulsen and Jacob 2004; Marotzke and Botzet 2007). One is the present-day climate with ice-cover only in the polar regions, the second is the so-called Snowball Earth climate with completely sea-ice covered oceans, potentially accompanied by glaciers on land. Below a certain level of atmospheric carbon dioxide or total solar irradiance (TSI), respectively, the present-day like mode disappears and the Snowball Earth mode is the only stable equilibrium (Budyko 1969; Sellers 1969). We will refer to this critical threshold as the Snowball Earth bifurcation point. Here, we use the state-of-the-art climate model ECHAM5/MPI-OM to study the transition from the present-day climate to a hypothetical modern Snowball Earth, which we define as the Earth in modern geography with complete sea-ice cover.

The Snowball Earth is of interest both from a geological as well as a climate modelling perspective. On the one hand, based on glacial deposits in Neoproterozoic ($\sim$750–550 Ma) rock sequences it has been argued that several Snowball Earth events might have occurred during Earth's history (Kirschvink 1992; Hoffman et al. 1998). On the other hand, the Snowball Earth challenges climate

modellers to confront their models and understanding of the climate system with the extreme climate of a Snowball Earth. Indeed, the work of Budyko (1969) and Sellers (1969), who used one-dimensional energy balance models and a temperature-dependent albedo parametrization to show that the entire Earth might become ice-covered if TSI was decreased by a few percent, stimulated a whole series of Snowball Earth modelling studies using the whole hierarchy of climate models, ranging from energy balance models (e.g., Held and Suarez 1974; North 1975), over Earth system models of intermediate complexity (e.g., Stone and Yao 2004; Donnadieu et al. 2004b; Romanova et al. 2006; Lewis et al. 2007), and atmosphere general circulation models with simplified ocean models (e.g., Jenkins and Frakes 1998; Chandler and Sohl 2000), to fully coupled atmosphere–ocean general circulation models (e.g., Poulsen et al. 2001; Poulsen and Jacob 2004). Some studies even incorporated dynamic ice sheet models (Hyde et al. 2000; Crowley et al. 2001; Peltier et al. 2004). Most studies attempted to estimate the Snowball Earth bifurcation point of the applied climate model by simulating the equilibrium climates for reduced values of TSI (justified by the "faint young sun" phenomenon) and/or reduced levels of atmospheric carbon dioxide. Several studies addressed the importance of various elements of the climate system such as ocean dynamics (Poulsen et al. 2001), surface winds (Poulsen and Jacob 2004), sea-ice dynamics (Lewis et al. 2007), sea-ice glaciers (Goodman and Pierrehumbert 2003; Pollard and Kasting 2005), and clouds (Le Hir et al. 2007; Poulsen and Jacob 2004), including their representation in the models.

However, except for the work of Donnadieu et al. (2004b), who used an Earth system model of intermediate complexity, previous studies focussed on whether a distinct combination of reduction in TSI and atmospheric carbon dioxide triggered a Snowball Earth, and they did not attempt to model the entire transition between the present-day like mode and the Snowball Earth mode. Instead of initializing the models from the present-day like mode, initial ocean temperatures were chosen to reduce the time required to reach equilibrium (see e.g. Poulsen and Jacob 2004). In contrast, we here start our simulations from the pre-industrial control climate of our climate model and apply an abrupt decrease of TSI or atmospheric CO_2 to trigger the transition to a modern Snowball Earth. We thereby follow the same experimental strategy as Marotzke and Botzet (2007), but we apply a wide range of TSI reductions instead of a single reduction of TSI to 0.01% of its today's value. In this study, we assess the following three issues.

First, we estimate both the Snowball Earth bifurcation point of the climate model ECHAM5/MPI-OM and the time needed to complete the transition from the present-day climate to a Snowball Earth. To our knowledge, there is only one study, with a simple energy balance model climate model, that estimates the transition time after a time-dependent reduction of TSI by 30% (Walsh and Sellers 1993).

Second, we analyze the response of the atmosphere and ocean heat transports and mean meridional circulation during the transition, with a focus on the Hadley cell and the Atlantic meridional overturning circulation. We compare our findings to the study of Donnadieu et al. (2004b) and find important differences.

Third, we study the degree of sea-ice cover that guarantees an unstoppable glaciation. This allows us to assess which extent of open equatorial water is possible, that is, whether our climate model exhibits solutions with near-complete sea ice cover but open equatorial waters.

The paper is organized as follows. Section 2 describes the climate model, and Sect. 3 the setup of the ECHAM5/MPI-OM simulations. Section 4 investigates the Snowball Earth bifurcation point. Section 5 presents a zero-dimensional energy balance model of the mean ocean potential temperature and compares the results of the climate model ECHAM5/MPI-OM with this zero-dimensional model. Section 6 analyzes the atmosphere and ocean meridional circulations and heat transports, followed in Sect. 7 by an investigation of the degree of sea-ice cover needed for an unstoppable glaciation. Section 8 gives a general discussion of the results, Sect. 9 follows with conclusions.

2 Model

We use the the Max Planck Institute for Meteorology coupled atmosphere–ocean general circulation model ECHAM5.3.02p2/MPI-OM-1.2.3p2 (labelled by ECHAM5/MPI-OM in the following). The atmosphere component ECHAM5 is the fifth generation of the ECHAM model series that originally evolved from the weather prediction model of the European Centre for Medium Range Weather Forecasts. The details of ECHAM5 are comprehensively described in Roeckner et al. (2003). ECHAM5 employs a dynamical spectral core with vorticity, divergence, temperature, and the logarithm of surface pressure being represented in the horizontal by a truncated series of spherical harmonics. In the vertical a hybrid sigma-pressure coordinate system is applied. The shortwave radiation scheme (Fouquart and Bonnel 1980) uses four spectral bands. For longwave radiation ECHAM5 employs the Rapid Radiative Transfer Model (RRTM) developed by Mlawer et al. (1997) with 16 spectral bands. ECHAM5 uses a stratiform cloud scheme including a cloud microphysical scheme and prognostic equations for the vapour, liquid, and ice phase, respectively. Snow at the surface and the inception of snow at the canopy

are modeled explicitly. Most important for our study is the treatment of surface albedo. The grid-mean surface albedo depends on a prescribed background albedo. Snow on land changes this background albedo according to the fractional snow cover of the grid cell. The fractional snow cover itself is a function of the snow depth measured in metres of water equivalent, but also of the orographic standard deviation so that sloping terrains require a larger snow depth than flat terrains to reach the same fractional snow cover. The albedo of snow on land depends on the land surface temperature and ranges from 0.3 at 0°C to 0.8 at or below –5°C. Moreover, the shielding effect of forests is accounted for in the surface albedo. In forest areas the surface albedo is further modified by snow cover on the canopy and the resulting canopy albedo.

The ocean component MPI-OM employs the primitive equations on an orthogonal curvilinear C-grid (Arakawa and Lamb 1977), with the North Pole shifted to Greenland to avoid a singularity at the geographical North Pole. The grid South Pole is located over Antarctica. In the vertical, the model employs unevenly spaced z-levels with the bottom topography being resolved by way of partial grid cells (Wolff et al. 1997). Technical details of MPI-OM can be found in Marsland et al. (2003). We here only give a short description of the embedded sea-ice model, which follows the dynamics of Hibler (1979) while the thermodynamics are incorporated by a zero-layer Semtner model relating changes in sea-ice thickness to a balance of radiant, turbulent, and oceanic heat fluxes (Semtner 1976). The freezing point of sea water is fixed to −1.9°C independent of salinity. Snow on ice is explicitly modeled, including snow/ice transformation when the snow/ice interface sinks below the sea level because of snow loading. The effect of ice formation and melting is accounted for by assuming a sea-ice salinity of 5. The albedo of bare sea ice depends on the ice surface temperature and ranges from 0.5 at 0°C to 0.75 at or below −1°C. Snow on sea ice leads to a significant albedo increase: if the water equivalent of snow depth is larger than 0.01 m, the sea ice is treated as being snow-covered. The albedo of snow-covered sea ice depends on the snow surface temperature and ranges from 0.6 at 0°C to 0.8 at or below −1°C. Sea ice thickness is limited to about 8 m, 75% of the thickness of the top layer of MPI-OM, to avoid the problem of dry model levels.

The atmosphere model ECHAM5 is coupled to the ocean model MPI-OM via the Oasis3 coupler (Valcke et al. 2003) with a coupling time step of one day. The ocean passes the sea surface temperature, sea-ice concentration and thickness, snow depth on ice, and ocean surface velocities to the atmosphere. The atmosphere provides the wind stress, heat flux, freshwater flux including river runoff and glacier calving, and 10 m wind speed to the ocean model. In the presence of sea ice the fluxes are calculated separately for sea-ice covered and open water parts of the grid cells. No flux adjustments are applied.

ECHAM5/MPI-OM has been extensively and successfully evaluated against observations (Hagemann et al. 2004; Jungclaus et al. 2006; Roeckner et al. 2006; Wild and Roeckner 2006) and was used for the integrations for the fourth assessment report of the Intergovernmental Panel on Climate Change (Brasseur and Roeckner 2005; Bengtsson et al. 2006; Landerer et al. 2007). Here, we use the low-resolution version of ECHAM5/MPI-OM to perform long simulations of up to 1,000 years length. The atmosphere component uses 19 vertical levels and has a horizontal resolution of T31 ($\sim$3.75°). The ocean model uses 40 vertical levels and has a horizontal resolution varying between 30 km near Greenland and 390 km in the tropical Pacific.

In contrast to most Snowball Earth model simulations, the location of continents, the mountain topography and the ocean bathymetry are all kept at their present-day values. Orbital parameters have modern values. Ozone follows the 1980–1991 climatology of Fortuin and Kelder (1998). Vegetation is prescribed according to a present-day climatology with monthly varying vegetation cover and leaf area indices for each surface grid cell. Land glaciers are fixed to their present-day extent. While the choice of modern boundary conditions inhibits the simulation of a Neoproterozoic Snowball Earth, it enables us to start our simulations from the present-day control climate and hence to simulate the entire transition from the present-day climate to a modern Snowball Earth. Atmospheric greenhouse gases are kept at pre-industrial levels (CO_2 = 286.2 ppm, CH_4 = 805.6 ppb, N_2O = 276.7 ppb, no cfc), except for one simulation where we set the atmospheric CO_2 concentration to 0.1% of its pre-industrial value, i.e., 0.2862 ppm. This will then be stated explicitly.

3 Setup of ECHAM5/MPI-OM simulations

We conduct two different sets of ECHAM5/MPI-OM simulations. In the first set, we estimate the Snowball Earth bifurcation point by starting from the present-day control climate of ECHAM5/MPI-OM (simulation CTRL with today's TSI, TSI_0 = 1,367 Wm^{-2}, and pre-industrial greenhouse gas levels) but decreasing TSI with respect to TSI_0. The model is run until it reaches a new equilibrium, which is either a modern Snowball Earth characterized by complete sea-ice cover or a climate with extended but not complete sea-ice cover. As a byproduct we also obtain the transition times to a modern Snowball Earth as a function of the reductions in TSI as well as the atmospheric and oceanic dynamics and heat transports during the entire

transition. We also conduct one experiment where we keep TSI at its present-day value but reduce atmospheric CO_2 to 0.1% of its pre-industrial value (simulation no CO_2). All simulations of this first set are summarised in Table 1.

In the second set of simulations, we investigate which degree of sea-ice cover guarantees an unstoppable glaciation. When the climate model is on the way to a modern Snowball Earth due to a decrease of TSI below the Snowball Earth bifurcation point, we increase TSI abruptly at different stages of sea-ice cover before the transition to a modern Snowball Earth is completed. This allows us to study the point of unstoppable glaciation that separates the present-day like states with partial sea-ice cover from Snowball Earth states with complete sea-ice cover. The different degrees of sea-ice cover are provided by simulation TSI91 (cf., Table 1). The simulations of the second set are summarised in Table 2, with the letter "R" indicating that these simulations are restarted from simulation TSI91 of the first set. Climate variables other than sea-ice cover, such as sea-ice thickness and mean ocean potential temperature, certainly also influence the response of the climate system to an increase of TSI. To account for this we also conduct two simulations where we set TSI back to 100% 1 and 2 years, respectively, before global sea-ice cover is completed in the simulation R2-TSI94. These two simulations marked by "RR" are included in Table 2.

4 Snowball Earth bifurcation point and transition time

We now describe the response of sea-ice cover to an abrupt decrease of TSI (cf., Fig. 1; Table 1). Setting TSI close to zero triggers global sea-ice cover within 14 years. All TSI values smaller than or equal to 91% TSI_0 lead to a modern Snowball Earth, but the transition time increases with TSI coming closer to TSI_0. For example, decreasing TSI to 50% leads to a modern Snowball Earth within 36 years, decreasing TSI to 75% leads to a modern Snowball Earth within 111 years, and decreasing TSI to 91% leads to a modern Snowball Earth within 480 years. The increase in global sea-ice cover accelerates strongly in time. In the simulation with 91% TSI_0, for example, freezing of the last 50% of the ocean only takes 45 years whereas freezing of the first 50% takes 431 years. Note that a modern Snowball Earth is also obtained by keeping TSI at 100% TSI_0 but setting the atmospheric CO_2 concentration to 0.1% of its pre-industrial level. The transition time for this virtually CO_2-free atmosphere is 240 years and hence between the transition times for TSI set to 75 and 87% TSI_0 with the atmospheric CO_2 kept at 100%.

In contrast, a reduction of TSI to 94% TSI_0 does not lead to global sea-ice cover within 1,000 years, but the sea-ice line shifts to 40°N/S with a very slow trend to increase. Given that 91% TSI_0 triggers a modern Snowball Earth but 94% does not, we find that the Snowball Earth bifurcation point in ECHAM5/MPI-OM is between 91 and 94% of the present-day total solar irradiance TSI_0.

Immediately after the reduction of TSI sea ice in the Southern Hemisphere decreases while the Northern Hemisphere sea ice does not show any initial dip. For TSI reductions below or equal to 50% TSI_0, sea ice then grows faster in the Northern Hemisphere than in the Southern Hemisphere due a deeper ocean bathymetry in the Southern Hemisphere. In contrast, for TSI reductions between 75 and 91% TSI_0, sea ice then grows faster in the Southern Hemisphere than in the Northern Hemisphere (not shown). An explanation for this will be given in Sect. 8. The Atlantic freezes over faster than the Pacific, with the time lag increasing from 3 months for the simulation TSI00 to 10 years for the simulation TSI91. Sea ice quickly becomes covered with snow, causing an albedo increase compared to bare sea ice by up to 0.1 in all simulations. In contrast, the formation of snow on land depends strongly on the TSI reduction. For simulations with drastic TSI reductions and hence shorter transition times, land snow cover is more spatially homogeneous but reaches lower maximum values.

Table 1 Summary of the first set of ECHAM5/MPI-OM simulations to study the response of the present-day climate to reductions in TSI

Simulation	TSI (%)	CO_2 (%)	Simulated years	Result
CTRL	100	100	100	Pre-industrial control simulation
TSI00	0.01	100	16	SE within 14a
TSI25	25	100	24	SE within 20a
TSI38	38	100	28	SE within 26a
TSI44	44	100	31	SE within 31a
TSI50	50	100	51	SE 37a
TSI75	75	100	151	SE 109a
TSI87	87	100	301	SE 285a
TSI91	91	100	501	SE within 480a
TSI94	94	100	1,000	sea-ice line at 40N/S after 1000a
noCO2	100	0.1	331	SE within 240a

The applied total solar irradiance is given in percentage of the present-day value 1,367 Wm^{-2}, the atmospheric carbon dioxide concentrations in percentage of its pre-industrial level 286.2 ppm

SE Snowball Earth

Table 2 Summary of the second set of ECHAM5/MPI-OM to investigate the point of unstoppable glaciation

Simulation	TSI (%)	CO_2 (%)	Restart from	Sea-ice cover at restart (December mean) (%)	Sim. years	Result
R1-TSI100	100	100	TSI91, year 478	87.7	72	Melting
R2-TSI94	94	100	TSI91, year 460	56.6	400	SE within 393a
R3-TSI94	94	100	TSI91, year 340	34.1	100	Melting
R4-TSI93	93	100	TSI91, year 460	56.6	60	SE within 52a
RR1-TSI100	100	100	R2-TSI94, year 850	81.7	60	Melting
RR2-TSI100	100	100	R2-TSI94, year 851	87.7	20	SE within 2a

The applied total solar irradiance is given in percentage of the present-day value 1,367 Wm^{-2}, the atmospheric carbon dioxide concentrations in percentage of its pre-industrial level 286.2 ppm, sea-ice cover in percentage of the global ocean area

SE Snowball Earth

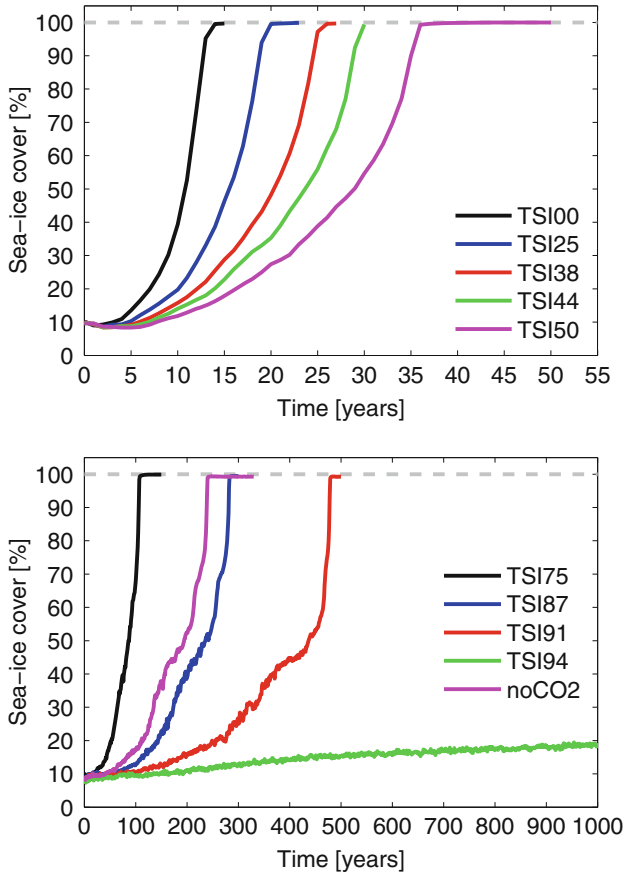

Fig. 1 Time evolution of sea-ice cover in percentage of global ocean area as a response to an abrupt decrease of TSI to 0.01–50% of its present-day value TSI_0 (*upper panel*) and 75–94% of the present-day TSI_0 (*lower panel*). The applied TSI value in percentage of the present-day TSI_0 is indicated by the last two digits in the simulation labels. The *lower panel* includes the simulation noCO2 for a virtually CO_2-free atmosphere. The *dashed gray lines* depict complete sea-ice cover and hence a Snowball Earth

For example, land snow cover at the end of simulation TSI00 exceeds 0.2 m water equivalent everywhere except in the the tropical regions of Africa, South America and China, whereas at the end of simulation TSI91, most land areas show no or only little snow cover (below 0.05 m water equivalent), and heavy snow cover of water equivalents of 1 m or more is restricted to the Himalaya, the Rocky Mountains, the Andes, and tropical Africa.

We now analyze the role of clouds and water vapor during the transition to a modern Snowball Earth as modelled in simulation TSI91. In the case of longwave radiation we can disentangle the radiative effect of clouds from the effect of water vapor by means of the all-sky and clear-sky radiation fluxes at the top of the atmosphere. These are simultaneously calculated in ECHAM5. During the transition the effective surface emissivity ϵ, defined as the ratio of outgoing all-sky longwave radiation at the top of atmosphere and the upward longwave radiation emitted by the Earth's surface, increases from 0.6 to 0.86, meaning a strong decline of the greenhouse effect, $g = 1 - \epsilon$, with the cooling of the Earth. The longwave effect of water vapour ($\epsilon_{\text{clearsky}}$,) can be disentangled from the effect of clouds (ϵ_{clouds},) by

$$\epsilon = \epsilon_{\text{clearsky}} + \epsilon_{\text{clouds}} = \text{LW}_{\text{TOA}}^{\text{allsky}} / \text{LW}_{\uparrow,\text{surface}} \quad (1)$$

with

$$\epsilon_{\text{clearsky}} = \text{LW}_{\text{TOA}}^{\text{clearsky}} / \text{LW}_{\uparrow,\text{surface}}. \quad (2)$$

Here, LW_{TOA} denotes the globally averaged annual longwave radiation at the top of the atmosphere with the superscripts marking the all-sky and the clear-sky fluxes. $\text{LW}_{\uparrow,\text{surface}}$ labels the globally averaged annual upward longwave radiation at the Earth's surface. Figure 2 shows that the effect of clouds on the effective surface emissivity stays constant during the entire transition to a modern Snowball Earth. The increase in the effective surface emissivity is indeed entirely caused by the increase in the clear-sky surface emissivity itself resulting from the decrease in atmospheric water vapour content (see Fig. 3). We also find the logarithmic dependence of the clear-sky greenhouse effect $g_{\text{clearsky}} = 1 - \epsilon_{\text{clearsky}}$ on the atmospheric water vapour content (Raval and Ramanathan

1989) over the whole range of water vapour content from 0.3 to 18 kg m^{-2} (not shown).

In the case of shortwave radiation the effect of clouds can be characterized by the difference of the all-sky planetary albedo $\alpha_{\mathrm{allsky}} = \mathrm{SW}^{\mathrm{allsky}}_{\uparrow,\mathrm{TOA}}/\mathrm{SW}_{\downarrow,\mathrm{TOA}}$ and the clear-sky planetary albedo $\alpha_{\mathrm{clearsky}} = \mathrm{SW}^{\mathrm{clearsky}}_{\uparrow,\mathrm{TOA}} / \mathrm{SW}_{\downarrow,\mathrm{TOA}}$ with the indices having the same meaning as in (1) and (2). Note that this difference is not equal to the albedo of clouds (Pierrehumbert 2002) although it quantifies the effect of clouds on the planetary albedo. During the transition to a modern Snowball Earth, clouds become less and less important for the reflection of shortwave radiation (see Fig. 4). This is a consequence of the strong increase in surface albedo with the advancement of sea ice, making the reflection of shortwave radiation by clouds dispensable.

In terms of cloud radiative forcing $\mathrm{CRF} = (\mathrm{LW}^{\mathrm{clearsky}}_{\mathrm{TOA}} - \mathrm{LW}^{\mathrm{allsky}}_{\mathrm{TOA}}) + (\mathrm{SW}^{\mathrm{allsky}}_{\mathrm{TOA}} - \mathrm{SW}^{\mathrm{clearsky}}_{\mathrm{TOA}})$, clouds cool the Earth during the entire transition by -18 W/m^2 during the first 300 years (see Fig. 5). From year 300 to the completion of sea-ice cover in year 480, the cloud radiative forcing declines to zero in year 480. The forcing over land increases from -10 Wm^{-2} during the first 190 years to 5 Wm^{-2} at year 480 when the transition to a Snowball Earth is completed. Over sea-ice free ocean areas, clouds have a large cooling effect that even increases during the transition. Shortly before sea-ice cover is complete the cloud forcing over open ocean areas declines to zero as no year-round sea-ice free ocean areas are left at this point. Ocean areas with more than 95% annual mean sea-ice cover experience an almost zero cloud radiative forcing. In contrast to the expectation of a small shortwave contribution but presumably still significant longwave contribution over sea ice, clouds over sea ice only exert a rather weak longwave forcing of about 8 Wm^{-2} in ECHAM5/MPI-OM. Also note after the transition, the cloud radiative forcing is slightly negative (-0.5 Wm^{-2}) due to negative cloud radiative forcing over sea ice.

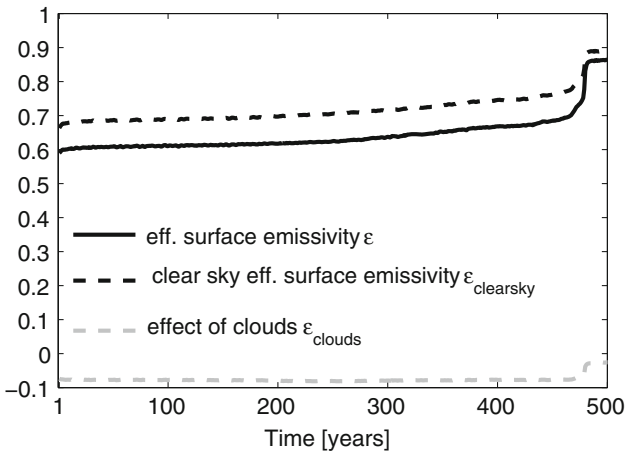

Fig. 2 Time evolution of the effective surface emissivity ϵ (*black solid*), the clear-sky effective surface emissivity $\epsilon_{\mathrm{clearsky}}$ (*black dashed*), and the effect of clouds (*gray dashed*) on the effective surface emissivity for a decrease of TSI to 91% of its present-day value (simulation TSI91)

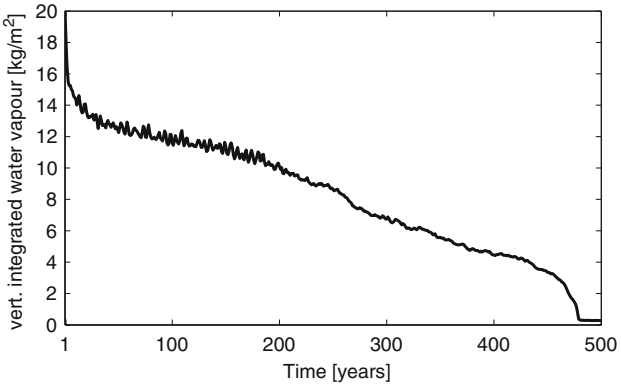

Fig. 3 Time evolution of the vertically integrated atmospheric water vapour for a decrease of TSI to 91% of its present-day value (simulation TSI91). Sea-ice cover is completed by year 480

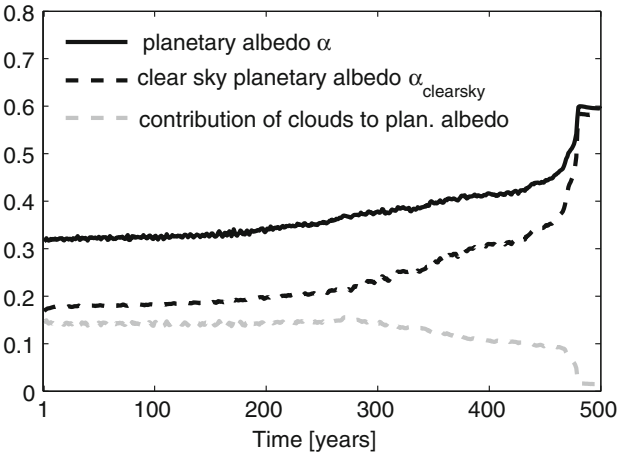

Fig. 4 Time evolution of planetary albedo (*black solid*), clear-sky planetary albedo (*black dashed*), and the effect of clouds on the planetary albedo as characterized by the difference of the planetary albedo and the clear-sky planetary albedo (*gray dashed*), for a decrease of TSI to 91% of its present-day value (simulation TSI91)

The analysis of the ocean heat flux for simulations with TSI set to 87, 91, and 94% TSI_0 shows a strong ocean heat loss directly after the TSI decrease (see Fig. 6). Then the ocean continues losing heat in all three simulations, but the rate of ocean heat loss decreases with time. For 87% TSI_0 it is still larger than 2 PW after 220 years. For 91% TSI_0 the ocean heat loss almost stabilizes near 1.5 PW, and its 15-year running mean never falls below 1 PW. The final freezing-over of the ocean is preceded by a strong pulse in ocean heat loss. In contrast, the simulation with 94% TSI_0 shows a monotonic decrease of ocean heat loss, which comes to close to zero after 1,000 years.

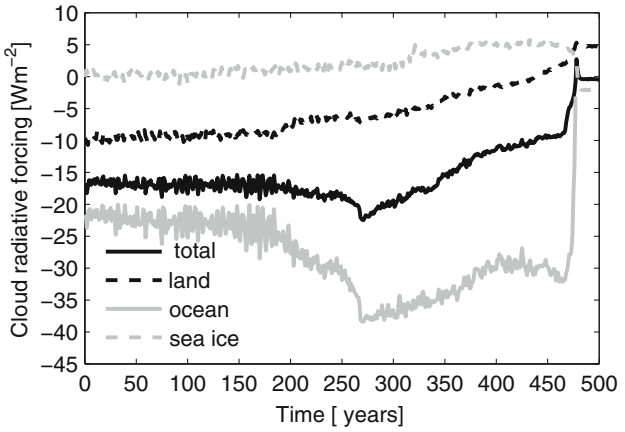

Fig. 5 Time evolution of the cloud radiative forcing for a decrease of TSI to 91% of its present-day value (simulation TSI91). Sea-ice cover is completed by year 480. When calculating the individual contribution of land, ocean and sea-ice areas, we dismissed "mixed" land–ocean cells. For the cloud radiative forcing over ocean areas, we only considered ocean cells with zero annual mean sea-ice cover. For the cloud radiative forcing over sea-ice areas, we only considered ocean cells with annual mean sea-ice cover greater than 95%

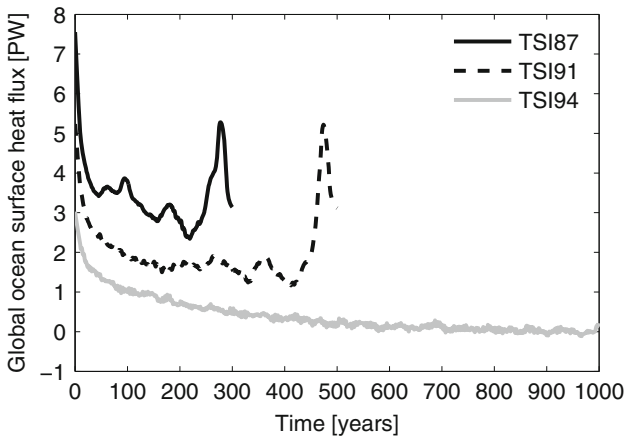

Fig. 6 Time evolution of global ocean heat loss for reductions of TSI to 87% (*black*), 91% (*black dashed*) and 94% (*grey*) of the present-day TSI_0. Positive values correspond to heat loss of the ocean, negative values to heat gain. A 15-year running mean is applied

The ocean eventually "decides" whether a given decrease of TSI triggers the transition to a modern Snowball Earth, since complete sea-ice cover requires not only the surface layers of the ocean to cool to close to the freezing point but also large parts of the underlying water column. For salinities >24.7 the density maximum of sea water is at its freezing point and the formation of sea ice at the surface must therefore be preceded by convection due to stability reasons (e.g., Washington and Parkinson 2005). This cooling of the ocean to close to the freezing point of sea water before the accomplishment of complete sea-ice cover is also seen in ECHAM5/MPI-OM (Fig. 7). That the freezing point in MPI-OM does not depend on the salinity but is fixed to −1.9°C is not a problem for the above mechanism as the vast majority of ocean areas have salinities greater than 24.7.

5 Comparison to a zero-dimensional energy balance model of mean ocean potential temperature

The ocean is by far the largest heat reservoir of the climate system and has to cool down to close to the freezing point before a modern Snowball Earth is possible. In the light of this outstanding role of the ocean, we devise a zero-dimensional energy balance model of the mean ocean potential temperature (shortly called energy balance model in the following). By modelling the response of the mean ocean potential temperature to a decrease in TSI, this energy balance model will allow us to estimate the transition time from the present-day climate to a modern Snowball Earth as well as the Snowball Earth bifurcation point.

We assume that the ocean is perfectly mixed in both the horizontal and the vertical directions. While this assumption is clearly daring for the present-day ocean, it becomes more and more reasonable as the Earth's climate approaches the Snowball Earth as described at the end of the preceding section. The energy balance model neglects the heat stored in the atmosphere and land components of the climate system.

In the energy balance model the heat flux at the ocean's surface is described by the (im)balance of shortwave and longwave radiation, and the mean ocean potential

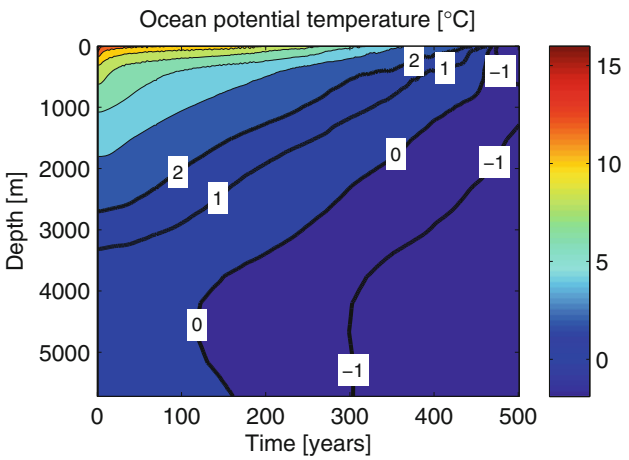

Fig. 7 Time evolution of horizontally averaged global ocean potential temperature in °C for a reduction of TSI to 91% of its present-day value (simulation TSI91). Contour intervals are 2°C for temperatures above 2°C and 1°C for temperatures below 2°C. The low-temperature region is highlighted with contour labels and thicker contour lines

temperature (referred to as ocean temperature in the following), θ, consequently obeys the budget equation

$$c\frac{d\theta}{dt} = \frac{(1-\alpha)}{4}\mathrm{TSI} - \epsilon\sigma\theta^4 \quad (3)$$

with c denoting the specific heat capacity of the ocean per unit area. Based on the MPI-OM parameters for the specific heat capacity of sea water, the density of sea water, and the global ocean volume and surface area, we obtain $c = 1.53 \times 10^{10}$ J K^{-1} m^{-2}. The exact value of c is not at all crucial for the results of the energy balance model though it ensures that the two tuning parameters α and ϵ take reasonable values. The parameter α models the reflection of solar radiation by clouds and by the ocean's surface and hence can be thought of as the planetary albedo. The parameter ϵ can be thought of as the effective surface emissivity and hence the efficiency of ocean heat loss by longwave radiation.

We use this energy balance model to predict the time evolution of the ocean temperature θ after an abrupt decrease of TSI. The model is only valid for ocean temperatures above the freezing temperature of sea water $\theta_\mathrm{f} = -1.9$°C. This is enough for our purposes here since we are only interested in the transition to a modern Snowball Earth, which in the energy balance model is defined by $\theta = \theta_\mathrm{f}$. The temperature of the present-day ocean is diagnosed from the control simulation CTRL to be $\theta_\mathrm{pd} = 4.35$°C and is used as the initial condition to (3). Requiring that the present-day ocean is a stable solution of (3) for the present-day $\mathrm{TSI}_0 = 1{,}367$ Wm^{-2}, the ratio of the two tuning parameters α and ϵ is fixed to

$$\frac{(1-\alpha)}{\epsilon} = 4\sigma\frac{\theta_\mathrm{pd}^4}{\mathrm{TSI}_0} \simeq 0.9838. \quad (4)$$

The value of ϵ is determined by demanding that the energy balance model matches the transition time of 14 years found in the ECHAM5/MPI-OM simulation TSI00. In this case, the solar radiation term in (3) can be neglected, and in conjunction with the initial condition $\theta = \theta_\mathrm{pd}$ and the constraint $\theta = \theta_\mathrm{f}$ for $t = 14$ years, we arrive at $\epsilon = 0.6736$. This fitted value of ϵ is taken to be constant for all TSI values. With (4) it follows that $\alpha = 0.3373$. In contrast to the energy balance models of Budyko and Sellers the albedo is held constant for all ocean temperatures between the freezing temperature of sea water and the present-day ocean temperature. Although we thus do not allow for an ice-albedo feedback in our energy balance model, this has the advantage that the estimate of the Snowball Earth bifurcation point gained with our energy balance model does not dependent on a chosen albedo parametrization as in the Budyko–Sellers models.

The fitted albedo of the energy balance model is close to the present-day planetary albedo, α_pd, which is estimated in the ECHAM5/MPI-OM control simulation CTRL to $\alpha_\mathrm{pd} = 0.326$. When comparing the effective surface emissivity of the energy balance model to the present-day effective surface emissivity ϵ_pd as modeled in the ECHAM5/MPI-OM control simulation CTRL, we need to include a form factor in ϵ_pd to incorporate that the sea surface temperature is larger than the vertically averaged mean ocean potential temperature used in the energy balance model to describe the energy loss by longwave radiation. With a present-day mean sea surface temperature of $\mathrm{SST}_\mathrm{pd} = 11.31$°C, a present-day mean ocean potential temperature $\theta_\mathrm{pd} = 4.35$°C, and a present-day mean effective surface emissivity $\epsilon_\mathrm{pd} = 0.583$ as estimated in the ECHAM5/MPI-OM control simulation CTRL, we arrive at a "corrected" value for the present-day effective surface emissivity of $\epsilon_\mathrm{pd}^\mathrm{corr} = \epsilon_\mathrm{pd}\,(\mathrm{SST}_\mathrm{pd}/\theta_\mathrm{pd})^4 = 0.644$ (with both θ_pd and SST_pd given in Kelvin). As for the albedo the effective surface emissivity of the energy balance model is thus close to its present-day value though slightly larger.

With these choices for α and ϵ, we use the energy balance model to estimate the transition time to a Snowball Earth as a function of decrease in TSI. This is done by solving (3) with the initial condition $\theta = \theta_\mathrm{pd}$ and the final condition $\theta = \theta_\mathrm{f}$. The resulting transition times are shown in Fig. 8 (gray line), which also includes the transition times found by the ECHAM5/MPI-OM simulations (black filled squares). The energy balance model is in good agreement with the ECHAM5/MPI-OM results for TSI values in the range of 0–50% TSI_0. This shows that TSI reductions to less than 50% are well described by radiative cooling of the ocean. In contrast, the energy balance model underestimates the transition times for the two TSI values 75% TSI_0 and 87% TSI_0. This underestimation is

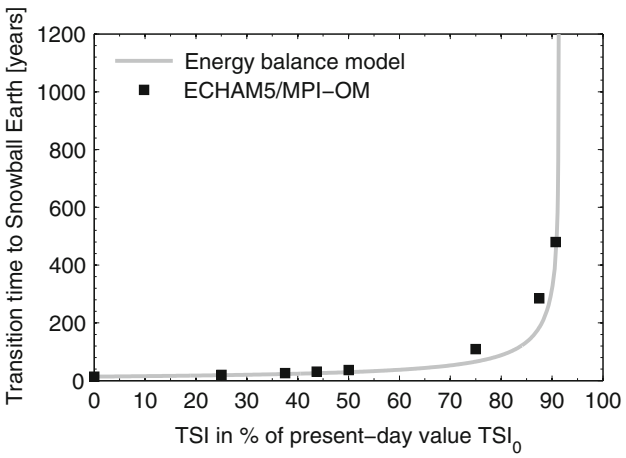

Fig. 8 Transition time from the present-day climate to a modern Snowball Earth in dependence of TSI given in percentage of its present-day value. *Black filled squares* denote the results of ECHAM5/MPI-OM simulations, the *gray line* denotes the transition time as modelled by the zero-dimensional energy balance model of the mean ocean potential temperature

somewhat surprising since one would expect that neglecting the ice-albedo feedback should result in an overestimation of the transition times compared to the ECHAM5/MPI-OM simulations. However, the energy balance model does not only miss the positive ice-albedo feedback, but also other processes that potentially could retard the transition, and these processes are only modelled by the value for ϵ tuned to the ECHAM5/MPI-OM simulation TSI00. The underestimation of the transition times in this range of TSI values might therefore indicate that delaying mechanism such as ocean dynamics as suggested by Poulsen et al. (2001) come into play for less drastic TSI reductions. For 91% TSI_0 the energy balance model is again in agreement with the ECHAM5/MPI-OM simulations. We interpret this agreement for 91% TSI_0 as a zero net effect of neglecting delaying mechanisms as well as the ice-albedo feedback in our energy balance model.

The energy balance model predicts that for TSI greater than 91.3% TSI_0 the ocean temperature never falls below the freezing temperature of sea water. This is expressed by the transition times becoming infinite above 91.3% TSI_0 (see Fig. 8). Although the energy balance model (EBM) itself does not experience a bifurcation at 91.3% TSI_0, we interpret this value as the EBM estimate of the Snowball Earth bifurcation point. This estimate is consistent with ECHAM5/MPI-OM giving a range of 91–94% TSI_0. We stress that the EBM estimate of the Snowball Earth bifurcation point does not depend on the individual values for α and ϵ, but only on their ratio in (4). On the one hand, this means that we could also tune α and ϵ to any ECHAM5/MPI-OM simulation with a TSI reduction below or equal to 91% TSI_0 without changing the EBM estimate of the Snowball Earth bifurcation point. On the other hand, if we chose a larger ratio, or equivalently a larger present-day ocean temperature θ_{pd}, the EBM estimate of the Snowball Earth bifurcation point would shift towards lower TSI. Therefore the present-day climate, represented in the energy balance model by the present-day ocean temperature, entirely controls the EBM estimate of the Snowball Earth bifurcation point through (4).

6 Atmosphere and ocean circulations and heat transports

We now study the atmosphere and ocean circulation both for a climate with extended but not complete sea-ice cover and for the entire transition period to a modern Snowball Earth. The focus will be on the Hadley cell in the atmosphere and the Atlantic meridional overturning circulation (AMOC). We also investigate atmosphere and ocean meridional heat transports and analyze how they are related to changes in the mean meridional circulation. For the atmosphere, we analyze the total advective heat transport and its decomposition in mean meridional and eddy transports. We use six-hourly instantaneous data and define the eddy terms as the deviation from the monthly and zonal mean. For the ocean, we report on the total ocean heat transport (calculated as the implied ocean heat transport based on monthly data of the heat and water fluxes at the ocean surface as well as monthly data of the ocean potential temperature) and the contribution of the meridional overturning circulation (calculated by monthly data of the horizontal velocity field and the ocean potential temperature). Moreover, we study the transport of latent heat due to sea-ice dynamics, which we calculate as the product of the transported sea ice volume times the melting enthalpy of sea-ice of 320×10^6 J m^{-3}.

We here analyze two simulations. First, we investigate the last 50 years of the simulation TSI94 as representative for an equilibrium climate with extended but not complete sea-ice cover. Second, we study the transient simulation TSI91 from the abrupt decrease of TSI to 91% until completion of sea-ice cover after 480 years.

We start with the analysis of the last 50 years of the simulation TSI94. The total advective atmospheric heat transport shown in Fig. 9 decreases in the Southern as well as the Northern Hemisphere with a decrease of the maximum heat transport around 35N/S by 0.8 PW. This decrease is mainly due to a decrease of eddy transport around 35N/S, which is caused by a decrease of eddy latent heat transport while the eddy dry static heat transport is virtually unchanged compared to the control simulation (not shown). The total heat transport by the mean meridional circulation changes very little, but this is a zero net effect of strong decreases in the magnitudes of the dry static heat transport and latent heat transport by the mean meridional circulation, which are opposite to each other. We see a weakening of the Hadley cell in the Southern Hemisphere and a break-down of the Ferrell cell in the Northern Hemisphere (not shown); however, the primary reason for the decrease in advective atmospheric heat transport are not changes in the atmospheric circulation but the strong decrease of atmospheric water vapour content by 55% compared to CTRL.

Global ocean heat transport decreases in TSI94 throughout the Northern Hemisphere, but stays constant in the Southern Hemisphere subtropical region and even increases in Southern Hemisphere midlatitudes (see Fig. 10). These changes in total ocean heat transport are mainly due to changes in the ocean heat transport due to the meridional overturning circulation (MOC, Fig. 10). The gyre transport comes close to zero polewards of 40N/50S due to the expansion of sea ice and intensifies slightly around the equator. The hemisphere-dependent behaviour of total ocean heat transport can be traced back to the

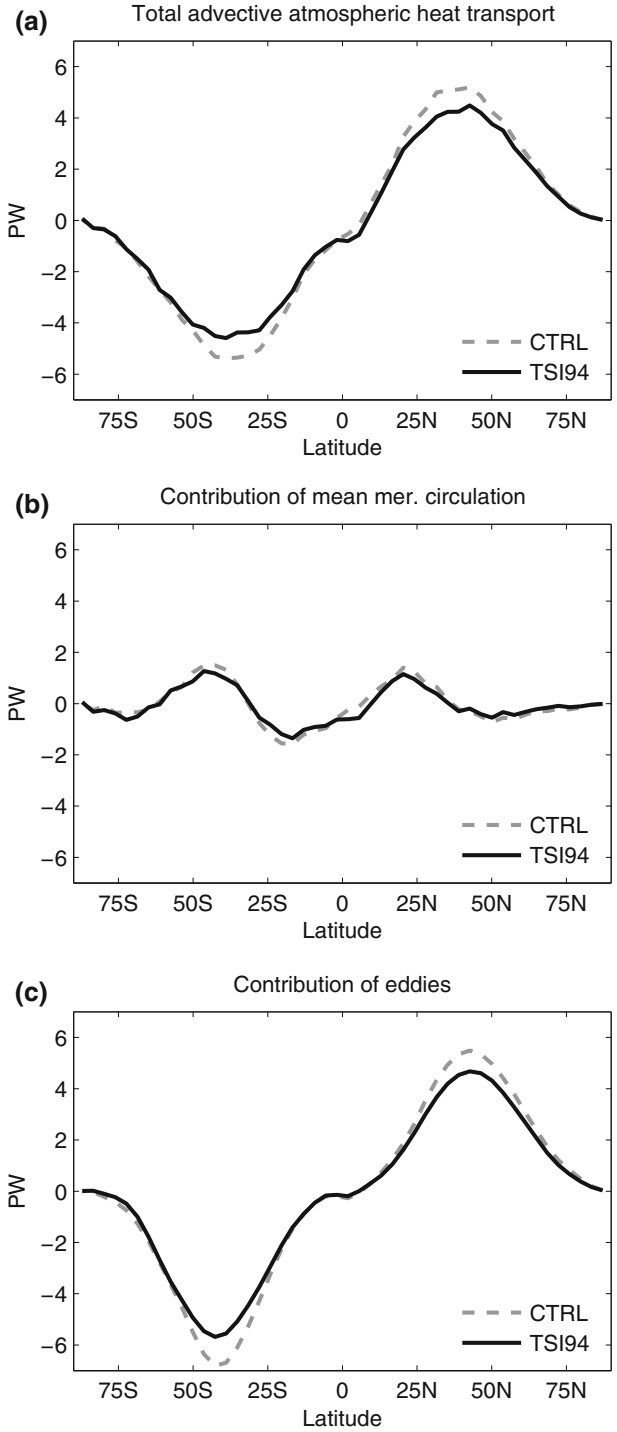

Fig. 9 **a** Total advective atmospheric heat transport, **b** contribution of the mean meridional circulation, and **c** contribution of eddies; for the control simulation CTRL (*gray dashed*) and averaged over the last 50 years of the simulation TSI94 (*black solid*)

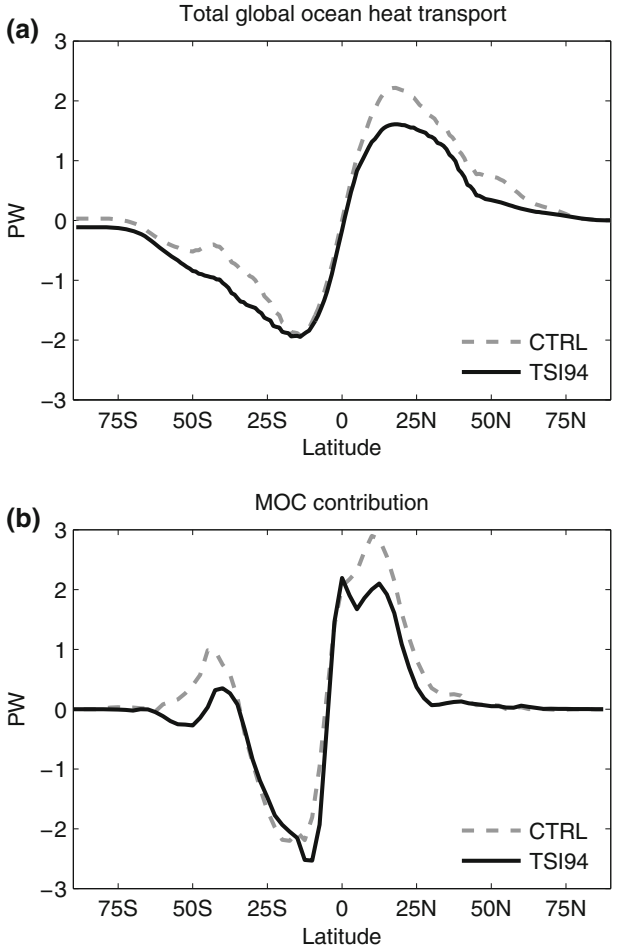

Fig. 10 **a** Total global ocean heat transport, and **b** contribution of the meridional overturning circulation (MOC); for the control simulation CTRL (*gray dashed*) and averaged over the last 50 years of the simulation TSI94 (*black solid*)

Atlantic while the total ocean heat transport in the Indo-Pacific Ocean shows a small decrease of its peak values around 15N/S in both hemispheres. Indeed, the present-day asymmetry of the AMOC, which in CTRL leads to northward ocean heat transport even in the Southern Hemisphere, is much weaker at the end of the simulation TSI94, and we even see a slight southward heat transport in the Southern Hemisphere. The AMOC shows a North Atlantic Deep Water (NADW) cell shallower and weaker by 7 Sv. In contrast the Antarctic Bottom Water (AABW) cell strengthens by 6 Sv and now extends up to 2,200 m instead of 2,700 m in CTRL. In the surface layers the wind-driven subtropical cells increase by 8–10 Sv in both hemispheres. At the end of the simulation TSI94 sea-ice transport contributes about 0.2 PW to the meridional transport of heat at 50N/60S, which is five times more than its maximum in CTRL (see Fig. 11).

Simulation TSI91 accomplishes a modern Snowball Earth within 480 years. Total advective atmospheric heat transport initially decreases slightly in both hemispheres, then increases slowly in the Southern Hemisphere after 200 years (Fig. 12). After 280 years, the peak value of heat transport in the Southern Hemisphere starts to shift

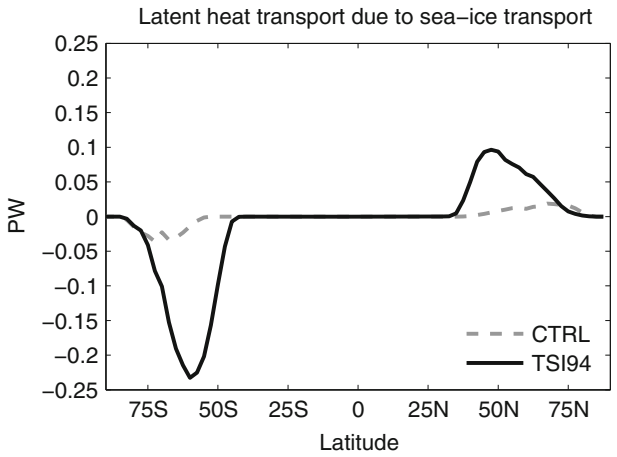

Fig. 11 Global ocean latent heat transport due to sea-ice transport in the control simulation CTRL (*gray dashed*) and averaged over the last 50 years of the simulation TSI94 (*black solid*)

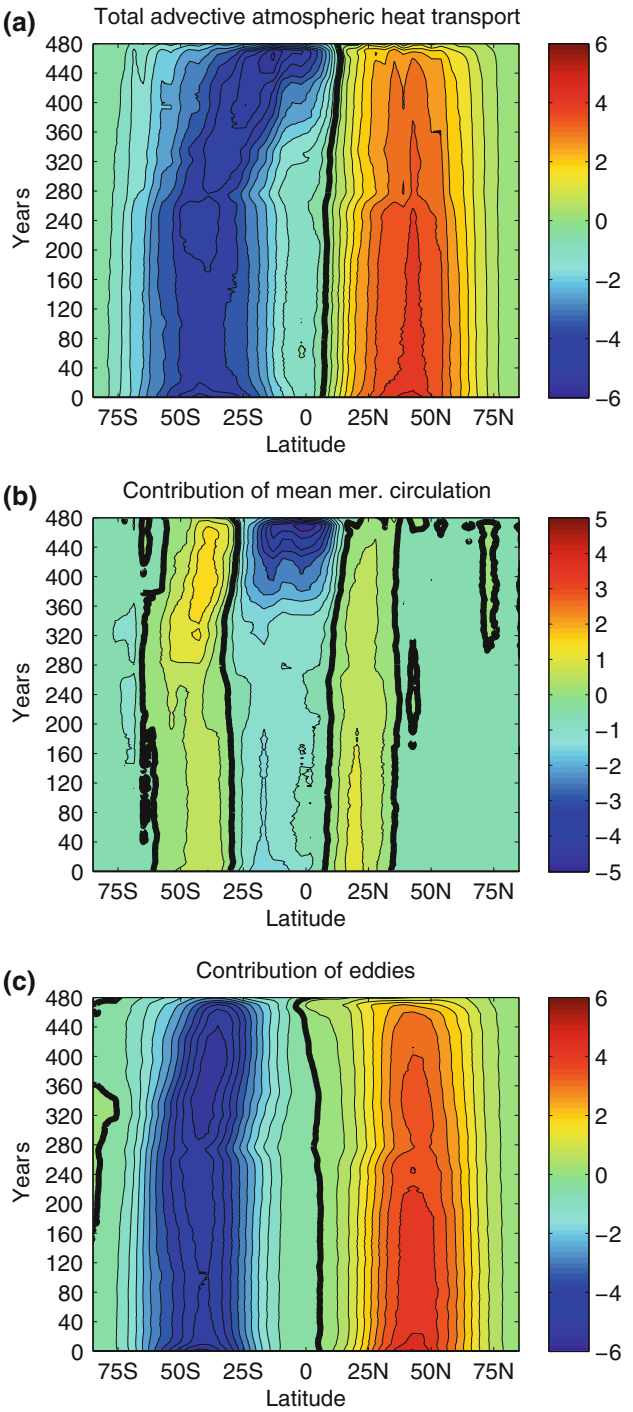

Fig. 12 Hovmoeller plot of **a** the total advective atmospheric heat transport, **b** the contribution of the mean meridional circulation, and **c** the contribution of eddies (all given in PW); for a reduction of TSI to 91% of its present-day value (simulation TSI91). The *thick black lines* display the zero contour level. Contour intervals are 0.5 PW. A 15-year running mean is applied. Sea-ice cover is completed by year 480

northwards. In contrast, the total advective atmospheric heat transport in the Northern Hemisphere continues to decline and hardly alters its meridional shape. This dominance of southward heat transport is due to large changes in the heat transport by the mean meridional circulation after year 300. At this moment the annual-mean heat transport by the mean meridional circulation resembles strongly the mean meridional heat transport during boreal summer (June, July, August) of CTRL. The changes in the heat transport by the mean meridional circulation are associated with substantial changes in the shape and magnitude of the Hadley cell. While the Hadley cell decreases in strength during the first 280 years in both hemispheres, its southern branch strongly intensifies after year 280 reaching a maximum strength of 41×10^{10} kg s^{-1} at year 467 and weakening shortly before the accomplishment of complete sea-ice cover (see Fig. 13). The eddy heat transport in TSI91 after 280 years exhibits a slight increase in the Southern Hemisphere and a decrease in the Northern Hemisphere but hardly changes its meridional shape with the advancement of sea-ice.

The total heat transport by the global ocean first increases after the abrupt decrease of TSI in TSI91 but shows a strengthening of southward heat transport in the Southern Hemisphere and a decrease of northward transport in the Northern Hemisphere after 200 years (see Fig. 14). This is also reflected in the contribution of the meridional overturning circulation showing a strong intensification of southward heat transport close to the equator after 250 years. The initial increase of northward heat transport in the Northern Hemisphere is related to an intensification of the NADW cell in the Atlantic. Figure 15 illustrates the time evolution of the peak values of the NADW cell and the AABW cell, which we define as the maximum (NADW) and minimum (AABW) values of the meridional overturning below 600 m, respectively. After the abrupt decrease of TSI, the NADW cell increases by 18 Sv in the first 50 years but then declines until the

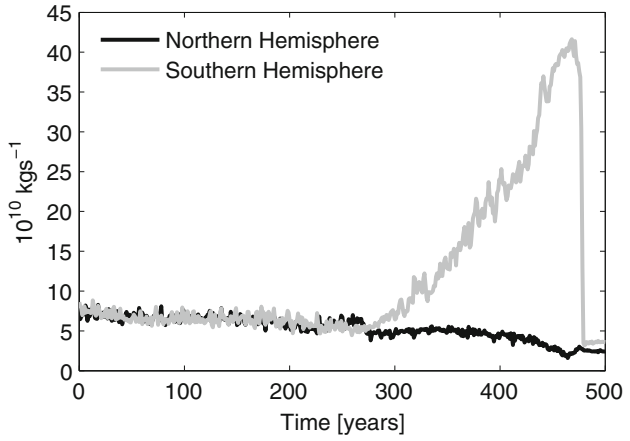

Fig. 13 Annual mean absolute maximum values of the Hadley cell branch in the Northern Hemisphere (*black*) and the Southern Hemisphere (*gray*) for a reduction of TSI to 91% of its present-day value (simulation TSI91)

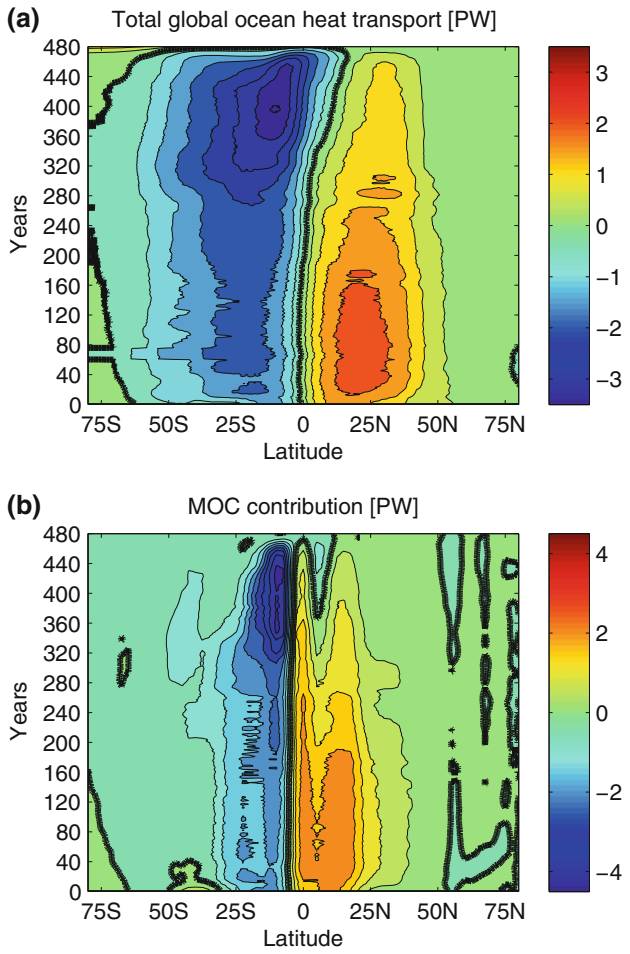

Fig. 14 Hovmoeller plot of **a** the total global ocean heat transport, and **b** the contribution of the MOC (both given in PW); for a reduction of TSI to 91% of its present-day value (simulation TSI91). The *thick black lines* display the zero contour level. Contour intervals are 0.5 PW. A 15-year running mean is applied. Sea-ice cover is completed by year 480

Atlantic becomes completely sea-ice covered in year 470. The AABW cell strengthens in the course of the simulation TSI91 until both cells decline after the completion of sea-ice cover in year 470 (upper panel of Fig. 15). The strength of the NADW and AABW cells are negatively correlated with a regime shift between year 290 and 312: the circulation changes from a strong NADW and weak AABW cell to a weak NADW and strong AABW cell (lower panel of Fig. 15). The regime shift in the NADW and AABW cells coincides with the increase of the southern branch of the Hadley cell. The wind-driven subtropical cells in the Atlantic do not show any immediate response to the abrupt decrease of TSI but slowly increase during the simulation and eventually are up to four times stronger than in CTRL (see Fig. 16). The strength of the clockwise northern cell and the anticlockwise southern cell are correlated although the southern cell intensifies by a factor of 4 while the northern cell only strengthens by a factor of less than two compared to CTRL. The regime shift from NADW to AABW as dominating AMOC cell is connected to the above-mentioned increase of southward ocean heat transport at this stage of the simulation TSI91. After 400 years the wind-driven subtropical cells in the Atlantic decline rapidly with the advancement of sea ice to the tropical Atlantic. In the Indo-Pacific the subtropical cells similarly intensify during the simulation with the southern cell even strengthening by a factor of 6 compared to CTRL around year 450 (not shown).

Poleward latent heat transport by sea ice increases significantly after 250 years and reaches a peak value of 1 PW in the Southern Hemisphere (see Fig. 17). However, the maximum sea-ice transport is not close to the equatorward edge of the sea-ice extent but centred around 40S.

7 Point of unstoppable glaciation

We will now turn to the second set of our experiments summarized in Table 2. At different stages of sea-ice cover of the simulation TSI91 we increase TSI to investigate which degree of sea-ice cover guarantees an unstoppable transition to a modern Snowball Earth, even if TSI is increased at this point (see Fig. 18). Setting TSI to 100% causes rapid melting of sea ice even for an almost completely frozen ocean with 87.7% sea-ice cover (simulation R1-TSI100). Although the Atlantic and the Indian Ocean are already completely covered with sea ice and only a narrow band of open water is left in the equatorial Pacific, sea-ice cover decreases rapidly after the increase of TSI to 100%. This picture is different if TSI is increased to less than 100%. Even if we start from simulation TSI91 with only 56.6% sea-ice cover, a TSI increase to 94% does not prevent a Snowball Earth but complete sea-ice cover is

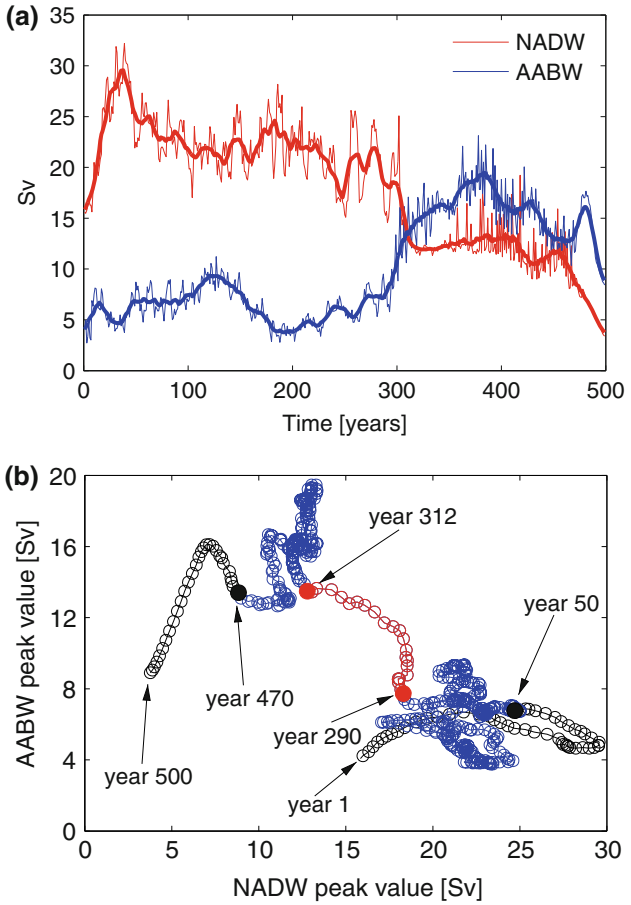

Fig. 15 **a** Time series of the absolute peak values of the NADW and AABW cells in the Atlantic for a reduction of TSI to 91% of its present-day value (simulation TSI91). The *thick lines* depict the 15-year running means. **b** Phase-space trajectory of the 15-year running means. Sea ice in the Atlantic is completed by year 470

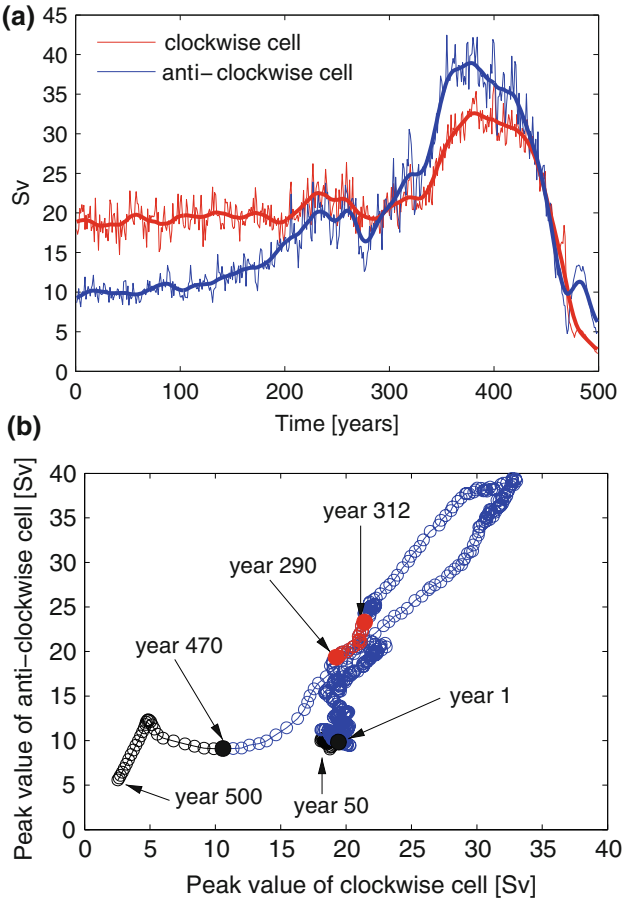

Fig. 16 **a** Time series of the absolute peak values of the wind-driven subtropical ocean overturning cells of the Atlantic for a reduction of TSI to 91% of its present-day value (simulation TSI91). The *thick lines* depict the 15-year running means. **b** Phase-space trajectory of the 15-year running means. Sea ice in the Atlantic is completed by year 470

realized within 393 years (simulation R2-TSI94). The intermediate state with constant sea-ice cover of 55% during 300 years but slow cooling of the ocean by a rate of 0.3 PW (corresponding to 0.8 Wm^{-2}) has a very sharp sea-ice edge at 10S showing almost no seasonal or interannual variability. In the Northern Hemisphere, the sea-ice edge is less uniform and shows more interannual and seasonal variability with sea ice reaching 30N in March and retreating to 55N in September in the North Pacific. That this intermediate state for 94% TSI_0 eventually freezes over implies that also for TSI values below 94% TSI_0, sea-ice cover above 56.6% is unstable and results in a modern Snowball Earth. This is confirmed by simulation R4-TSI93. Increasing TSI to 94% at 34.1% sea-ice cover in the simulation TSI91 leads to melting of sea ice with sea-ice cover after 100 years being close to that at the end of simulation TSI94. This implies that if we start from the present-day control climate and reduce TSI to values between 94 and

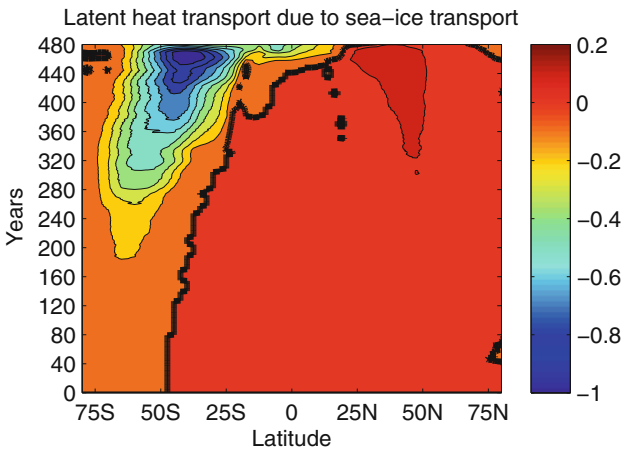

Fig. 17 Hovmoeller plot of the latent heat transport due to sea-ice transport in PW for a reduction of TSI to 91% of its present-day value (simulation TSI91). Contour intervals are 0.1 PW. A 15-year running mean is applied

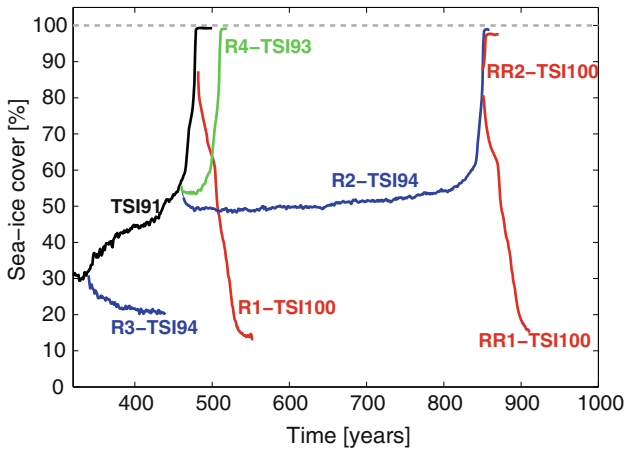

Fig. 18 Response of sea-ice cover in percentage of ocean area after an increase of TSI at different stages of the simulation TSI91 (*black*). *Green* means an increase of TSI to 93%, *blue* an increase of TSI to 94%, and *red* an increase of TSI to 100% of its present-day value. The plot also includes two simulations where we set TSI back to 100% one year before complete sea-ice cover is accomplished in the simulation R2-TSI94. The simulations can be identified by the labels attached to the lines of sea-ice cover evolution (cf. Tables 1, 2)

100% TSI_0, sea-ice cover will not exceed 34.1% in ECHAM5/MPI-OM. Assuming that ECHAM5/MPI-OM does not exhibit an additional stable mode between the present-day like and the Snowball Earth mode, we conclude that stable states can have no greater than 56.6% sea-ice cover.

To study the extent to which the point of unstoppable glaciation for 100% TSI_0 depends on sea-ice thickness and mean ocean potential temperature, we conduct the simulations RR1-TSI100 and RR2-TSI100 where we set TSI back to 100% shortly before global sea-ice cover is realized in the simulation R2-TSI94. Increasing TSI to 100% prevents the transition to a Snowball Earth for a sea-ice cover of 81.7% (simulation RR1-TSI100) but does not inhibit complete sea-ice cover for a slightly higher sea-ice cover of 87.7% (simulation RR2-TSI100). The simulation RR2-TSI100 starts from the same degree of sea-ice cover as the simulation R1-TSI100, but sea-ice is 0.5 m thicker and the ocean is 0.42 K colder than for the experiment R1-TSI100 (see Table 3). While it is not surprising that the point of unstoppable glaciation is shifted to smaller degrees of sea ice cover with lower ocean temperatures and thicker sea ice, we can estimate a lower bound for the point of unstoppable glaciation for 100% TSI_0. As ECHAM5/MPI-OM at the beginning of the simulation RR1-TSI100 is already close to the maximum value of sea-ice thickness of 8 m and minimum value of mean ocean potential temperature of −1.9°C, the point of unstoppable glaciation for 100% TSI_0 should be above 80% sea-ice cover, independent of the explicit state chosen to set TSI back to 100%. Together with the simulations R2-TSI94 and R3-TSI94 showing that the point of unstoppable glaciation for 94% TSI_0 is below 56.6% sea-ice cover, this demonstrates a strong dependence of the point of unstoppable glaciation on TSI.

The classical energy balance models of Budyko (1969) and Sellers (1969) describe the climate only in terms of sea-ice cover and neglect other variables of the climate system. This is certainly an oversimplification of the ECHAM5/MPI-OM model as well as the "true" climate system. We now analyze how strong this simplification is in the case of ECHAM5/MPI-OM, by investigating the correlation of mean ocean potential temperature and sea-ice cover for various ECHAM5/MPI-OM simulations (see Fig. 19). If the energy balance models, and hence the Budyko–Sellers diagram, were a complete description of the ECHAM5/MPI-OM model, all simulations would give exactly the same mean ocean potential temperature for the same sea-ice cover indicating that sea-ice cover completely describes the state of the climate system. Indeed, all simulations of the transition from the present-day climate to a modern Snowball Earth triggered by an abrupt decrease of TSI (cf. Table 1) roughly show the same dependence of mean ocean potential temperature on sea-ice cover. Note that simulations of the first set not included in Fig. 19 fall in the region covered by the selected simulations shown in Fig. 19. This shows that sea-ice cover is a sufficient description of the climate state of ECHAM5/MPI-OM when the climate model evolves from the present-day climate into a modern Snowball Earth. The physical reason here is that the formation of sea ice requires that most parts of the underlying water column are cooled to close to the freezing point (see Sect. 4). In contrast, the simulation R1-TSI100 (cf. Table 2) is not in accordance with the above correlation of mean ocean potential temperature and

Table 3 Summary of sea-ice cover in percentage of the total ocean area, mean sea-ice thickness and mean ocean potential temperature before the increase of total solar irradiance to 100% for three simulations of the second set of ECHAM5/MPI-OM simulations

Simulation	Sea-ice cover at restart (December mean) (%)	Sea-ice thickness at restart (December mean) (m)	Mean ocean temperature at restart (annual mean) (K)	Result
R1-TSI100	87.7	5.98	271.94	Melting
RR1-TSI100	81.7	6.12	271.54	Melting
RR2-TSI100	87.7	6.48	271.52	SE within 2a

SE Snowball Earth

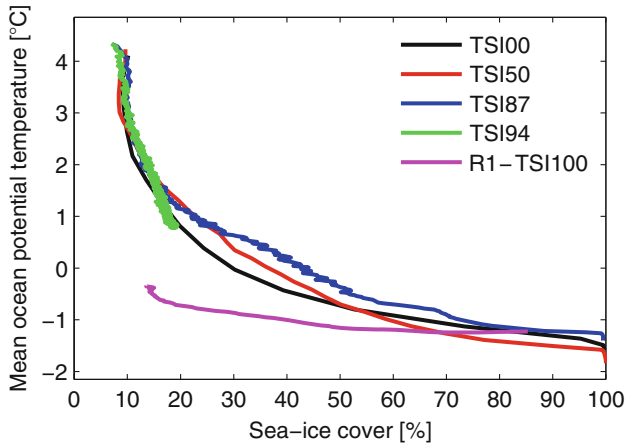

Fig. 19 Annual mean ocean potential temperature in dependence of sea-ice cover for four simulations applying an abrupt decrease of TSI (*black*, *red*, *blue*, *green*) and one simulation where we increased TSI to 100% shortly before sea-ice cover is complete (*magenta*)

sea-ice cover, because melting of sea ice only requires to warm the ocean surface layers and hence leaves the mean ocean potential temperature largely unaffected.

8 Discussion

In the coupled atmosphere–ocean general circulation model ECHAM5/MPI-OM, the Snowball Earth bifurcation point for the transition to a Snowball Earth is in the range of 91 to 94% of today's TSI. This is in agreement with the FOAM atmosphere–ocean general circulation model despite differences in the applied geography (Poulsen and Jacob 2004).

The transition times to a Snowball Earth have only been studied with a simple climate model (Walsh and Sellers 1993); a time-dependent decrease of TSI by 30% over 90 years resulted in a Snowball Earth within 81 years. This is broadly consistent with our simulation with 75% TSI_0 giving a transition times of 109 years, although the simplicity of this earlier model and the different strategy of TSI decrease render a comparison difficult.

In contrast to a previous study with the Earth system model of intermediate complexity PUMA (Romanova et al. 2006), our model ECHAM5/MPI-OM is very sensitive to a decrease in atmospheric carbon dioxide. When we remove virtually all carbon dioxide from the atmosphere, the Earth freezes over even with 100% TSI_0. While the sole radiative effect of CO_2 is too small to trigger a Snowball Earth, removing CO_2 activates the ice-albedo and water-vapor feedbacks. In contrast to the Snowball Earth literature, which almost exclusively focuses on the ice-albedo feedback alone, we find that the water-vapor feedback is also key to the initiation of a Snowball Earth, as seen by the strong increase in the clear-sky emissivity (see also Pierrehumbert 2002 and Fraedrich 1979). We speculate that ECHAM5/MPI-OM has less difficulties generating a Snowball Earth partly due to a strong water-vapor feedback in our model, consistent with ECHAM5/MPI-OM simulations of the Paleocene–Eocene (55 Ma BP) presented in Heinemann et al. (2009). There, strong reduction in the clear-sky surface emissivity are key to explain the high climate sensitivity of those simulations, and the water-vapor feedback is thought to be one of the main reason for the simulated reduction in clear-sky surface emissivity. Clouds in ECHAM5/MPI-OM always exert a negative radiative forcing, even above completely sea-ice covered regions. This is in contrast to the results of Poulsen and Jacob (2004) and makes clear that clouds are an important point of discrepancy between models (see also Le Hir et al. (2007) for the influence of clouds on the deglaciation threshold of a Snobwall Earth).

Our analysis of the climate with sea ice extended to 40N/S due to a decrease of TSI to 94% shows a decrease of atmospheric heat transport compared to the present-day control simulation CTRL. In the literature, there is only a single study that systematically investigates the response of atmospheric heat transport to sea-ice expansion. Using the CLIMBER-2 model with a Neoproterozoic continental reconstruction, Donnadieu et al. (2004b) found that a decrease of atmospheric carbon dioxide from 3,500 to 500 ppm caused an expansion of sea ice from 60N/S to 40N/S. These simulations should therefore be comparable to our present-day control simulation CTRL and our simulation TSI94 with 94% TSI_0. While in CLIMBER-2 sea-ice expansion lead to an increase of atmospheric heat transport in both its mean meridional and eddy components, our simulations suggest the completely opposite. We find a decrease in atmospheric heat transport, which is entirely due to a decrease of atmospheric eddy heat transport. This questions the conclusion in Donnadieu et al. (2004b) that atmospheric heat transport represents a negative feedback working against sea-ice advance, and illustrates that the role of atmospheric heat transport during the transition to a Snowball Earth is still unclear. Concerning the ocean heat transport, we find similar hemisphere-dependent changes as in Donnadieu et al. (2004b).

Why do we see an intensification of southward and a decline of northward atmospheric and oceanic heat transports as sea ice comes close towards the equator? The answer lies in the present-day asymmetric distribution of the continents. In ECHAM5/MPI-OM, sea-ice covered ocean areas have a substantially higher albedo than frozen land areas because of two reasons. First, the albedo of snow-free land largely depends on the assumed background albedo, which is in the range of 0.1 to 0.3 for most land areas. This is much lower than the albedo of sea ice. Second, snow causes less albedo increase on land than on sea ice, since snow on land has a lower minimum albedo

than snow on sea-ice, and the albedo effect of snow on land is further diminished by the shielding effect of forests as well as the effect of decrease in fractional snow cover as a consequence of sloping terrain. This difference in the albedo of sea-ice areas and frozen land areas results in a larger surface albedo in the Southern than the Northern Hemisphere after year 240 for a reduction of TSI to 91% of its present-day value (see Fig. 20). Consequently, the Southern Hemisphere receives less shortwave radiation than the Northern Hemisphere, and this deficit must be balanced by anomalous southward heat transport, compared to the present-day climate. This also explains the faster expansion of sea ice in the Southern Hemisphere seen for the simulations with 75 to 91% TSI_0 (cf., Sect. 4).

How do our simulations then help us understand the role of atmosphere and ocean heat transports and dynamics? First, we can say with confidence that the wind-driven meridional overturning circulation intensifies strongly during the transition and hence becomes more and more important for meridional ocean heat transport as sea ice spreads towards the equator. This is in agreement with a previous sensitivity study with an atmosphere–ocean general circulation model that showed that the wind-driven ocean circulation is an important factor to make global glaciation more difficult (Poulsen and Jacob 2004). Second, we also see the importance of sea-ice dynamics in our simulations, in accordance with Lewis et al. (2003, 2007). Meridional sea-ice transport not only leads to poleward latent heat transport and hence a cooling of the open water regions, but it also cools the preciously open water regions by the high albedo of the exported sea ice. Third, we see a strong intensification of the Hadley cell when sea ice enters the tropical region, and a weakening of the Hadley cell just prior to the accomplishment of final glaciation, again in accordance with Poulsen and Jacob (2004). The simultaneous increase of southward heat transport in the tropics by the mean meridional circulations in the atmosphere and the ocean reflects the strong coupling between both mechanisms (cf., Held 2001). A stronger Hadley cell means stronger surface winds and consequently an increase in the wind-driven subtropical ocean cells. This confirms the peculiar role of surface winds that has also been recognized in previous studies (Poulsen and Jacob 2004; Lewis et al. 2003, 2007).

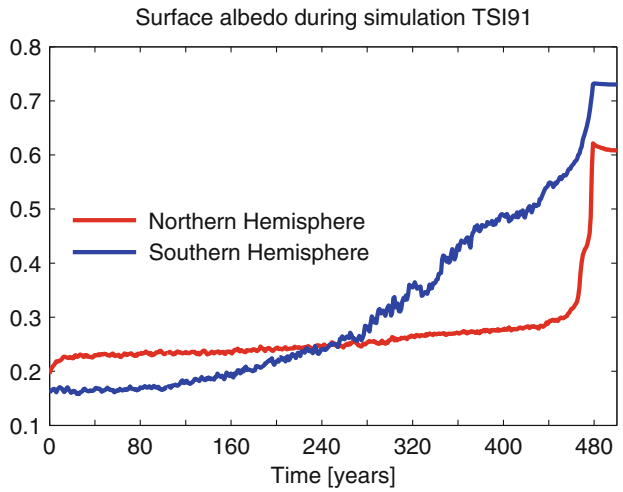

Fig. 20 Surface albedo of the Northern and Southern Hemisphere during the transition to a modern Snowball Earth triggered by a reduction of TSI to 91% (simulation TSI91). Sea-ice cover is completed by year 480

While the existence of the point of unstoppable glaciation and hence a runaway ice-albedo feedback is inevitable as soon as the meridional heat transport is nonzero (Held and Suarez 1974), it is a priori unknown where this point is located. For 100% TSI, we find that this point should be above 80% sea-ice cover, which is much closer to complete sea-ice cover than the position of the unstable branch in classical energy balance models (e.g., North 1975). The melting of a near-Snowball Earth in Poulsen (2003) is consistent with our simulations for an increase of TSI to 100% TSI_0. However, this alone does not justify the conclusion of a weak runaway ice-albedo feedback for Neoproterozoic boundary conditions drawn in Poulsen (2003) due to the strong dependence of the point of unstoppable glaciation on TSI found in our study.

In ECHAM5/MPI-OM there is no TSI value resulting in stable climates with sea-ice cover above 56.6%, i.e. we do not find stable states with near-complete sea ice cover but open equatorial waters. This is in contrast to Poulsen and Jacob (2004) who find that 65% sea-ice cover is stable in the FOAM model. Obvious reasons for this discrepancy are differences in the cloud radiative forcing above sea ice (close to zero in ECHAM5/MPI-OM, but about 30 Wm^{-2} in FOAM) and missing sea-ice dynamics in FOAM. Differences in the strength of the water-vapor feedback and different values for sea-ice albedo might also be important, but a comparison is hindered as Poulsen and Jacob (2004) do not provide data for these variables. To judge whether differences in the applied geography (modern in our study, but equatorial supercontinent in Poulsen and Jacob 2004) are important for the differences in the stability threshold would require to repeat our simulations with Neoproterozoic continents, which is beyond the scope of this study. There are nonetheless two interesting issues regarding the location of continents. First, the strong southward heat transport seen in our study clearly is a consequence of choosing modern continents due to the vastly different albedo of ocean, sea ice, and land. Second, it recently has been demonstrated that ocean heat transport plays a major role in setting the latitude of the sea-ice edge (Rose and Marshall 2009; Ferreira et al. 2009) as sea ice tends to rest at minima of ocean heat transport, and that the structure of meridional ocean heat

transport itself is sensitive to continental boundaries (Enderton and Marshall 2009). Altogether, this proposes a new and yet unexplored mechanism of how the location of continents might influence the stability threshold.

ECHAM5/MPI-OM neither includes a dynamic vegetation nor an ice sheet model. The use of a vegetation mask fixed to the present-day climate results in too low land albedos for regions with present-day forest cover like Siberia or the tropical rain forest regions due to the shielding effect of forests. The same is true for the lack of a dynamic ice sheet model although we consider it to be less important for our study as most of our simulations are rather short. Finally, the restriction of sea-ice thickness to about 8 m in MPI-OM to avoid dry model layers introduces an artificial heating source below the sea ice. Altogether, these three deficits bias our model results to an overestimation of the transition times. Similarly, the estimated range of the Snowball Earth bifurcation point would shift to higher TSI values if these three deficits were removed. They should be addressed when one attempts to simulate the equilibrium climate of a Snowball Earth, but we here consider them not to be of first order for modelling the transition from the present-day climate to a Snowball Earth. Apart from the transition to a modern Snowball Earth, including an ice sheet model would allow us to test the existence of "oasis" solutions in an atmosphere–ocean general circulation model. These "oasis" solutions, found in an energy balance model coupled to an ice sheet model (Crowley et al. 2001; Peltier et al. 2004, 2007), exhibit tropical land glaciers while tropical oceans remain sea-ice free and are located in between the present-day like mode and the Snowball Earth mode in plots of global surface temperature versus TSI or longwave CO_2 forcing.

We have only modelled the physical climate system comprising atmosphere, ocean, and sea ice. Atmospheric carbon dioxide levels are fixed in our study. It is certainly interesting to include the interactions of climate and carbon dioxide in Snowball Earth simulations. For example, the continental break-up of Rodinia was shown to trigger a Snowball Earth due to an increase in runoff and due to basaltic traps in the GEOCLIM model (Donnadieu et al. 2004a; Godderis et al. 2007). Moreover, it has been suggested that including the Neoproterozoic carbon cycle proposed by Rothman et al. (2003) may inhibit global glaciations (Peltier et al. 2007) though this is still a matter of debate (Godderis and Donnadieu 2008; Hoffman et al. 2008; Peltier and Liu 2008). We leave these issues for future research.

9 Conclusions

Based on our simulations with the coupled atmosphere–ocean general circulation model ECHAM5/MPI-OM to study the transition from the present-day climate to a modern Snowball Earth, we conclude the following:

1. The Snowball Earth bifurcation point of ECHAM5/MPI-OM is between 91 and 94% of the present-day total solar irradiance (TSI), in agreement with the FOAM atmosphere ocean general circulation model (Poulsen and Jacob 2004). The transition time from the present-day climate to a modern Snowball Earth increases from 14 years for virtually switching off the sun to 480 years for decreasing TSI to 91% of its present-day value.
2. The Snowball Earth bifurcation point and the transition time found with ECHAM5/MPI-OM are well reproduced with a zero-dimensional energy balance model of the mean ocean potential temperature.
3. The asymmetric distribution of continents between the Northern and Southern Hemisphere causes strong heat transports toward the more water-covered Southern Hemisphere as sea ice spreads towards the equator. The southern Hadley cell and the wind-driven subtropical ocean cells strengthen by a factor of 4 as sea-ice approaches the equator.
4. For 100% TSI the point of unstoppable glaciation is much closer to complete sea-ice cover than in classical energy balance models. Stable states have no greater than 56.6% sea-ice cover implying that ECHAM5/MPI-OM does not exhibit stable states with near-complete sea-ice cover but open equatorial waters.

Acknowledgments We thank two anonymous referees for their comments. We are indebted to Erich Roeckner, Michael Botzet, Dirk Notz and Uwe Mikolajewicz for discussions and proof-reading. We also thank Michael Botzet for technical help when performing the simulations. The energy balance model was inspired by discussions with Martin Stier and Niko Sandschneider. This work was supported by the Max Planck Society and the International Max Planck Research School on Earth System Modelling. All simulations were performed at the German Climate Computing Center (DKRZ) in Hamburg, Germany.

Open Access This article is distributed under the terms of the Creative Commons Attribution Noncommercial License which permits any noncommercial use, distribution, and reproduction in any medium, provided the original author(s) and source are credited.

References

Arakawa A, Lamb VR (1977) Computational design of the basic dynamical processes of the UCLA general circulation model. Methods Comput Phys 17:173–265

Bengtsson L, Hodges KI, Roeckner E (2006) Storm tracks and climate change. J Clim 19(15):3518–3543

Brasseur GP, Roeckner E (2005) Impact of improved air quality on the future evolution of climate. Geophys Res Lett 32(23):L23704

Budyko MI (1969) Effect of solar radiation variations on climate of Earth. Tellus 21(5):611–619
Chandler MA, Sohl LE (2000) Climate forcings and the initiation of low-latitude ice sheets during the Neoproterozoic Varanger glacial interval. J Geophys Res Atmos 105(D16):20737–20756
Crowley TJ, Hyde WT, Peltier WR (2001) CO_2 levels required for deglaciation of a "Near-Snowball" Earth. Geophys Res Lett 28(2):283–286
Donnadieu Y, Godderis Y, Ramstein G, Nedelec A, Meert J (2004a) A 'snowball Earth' climate triggered by continental break-up through changes in runoff. Nature 428(6980):303–306
Donnadieu Y, Ramstein G, Fluteau F, Roche D, Ganopolski A (2004b) The impact of atmospheric and oceanic heat transports on the sea-ice-albedo instability during the Neoproterozoic. Clim Dyn 22(2–3):293–306
Enderton D, Marshall J (2009) Controls on the total dynamical heat transport of the atmosphere and oceans. J Atmos Sci (to appear)
Ferreira D, Rose B, Marshall J (2009) In preparation
Fortuin JPF, Kelder H (1998) An ozone climatology based on ozonesonde and satellite measurements. J Geophys Res Atmos 103(D24):31709–31734
Fouquart Y, Bonnel B (1980) Computations of solar heating of the earth's atmosphere: A new parametrization. Beitr Phys Atmos 53:35–62
Fraedrich K (1979) Catastrophes and Resilience of a zero-dimensional climate system with ice-albedo and greenhouse feedback. Q J R Meteorol Soc 105(443):147–167
Godderis Y, Donnadieu Y (2008) Carbon cycling and snowball Earth. Nature 456(7224)
Godderis Y, Donnadieu Y, Dessert C, Dupre B, Fluteau F, Francois LM, Meert J, Nedelec A, Ramstein G (2007) Coupled modeling of global carbon cycle and climate in the Neoproterozoic: links between Rodinia breakup and major glaciations. Comptes Rendus Geoscience 339(3-4):212–222
Goodman JC, Pierrehumbert RT (2003) Glacial flow of floating marine ice in "Snowball Earth". J Geophys Res Oceans 108(C10):3308
Hagemann S, Machenhauer B, Jones R, Christensen OB, Deque M, Jacob D, Vidale PL (2004) Evaluation of water and energy budgets in regional climate models applied over Europe. Clim Dyn 23(5):547–567
Heinemann M, Jungclaus J, Jochem M (2009) Warm Paleocene/Eocene climate as simulated in ECHAM5/MPI-OM. Clim Past Dis 5:1297–1336
Held IM (2001) The partitioning of the poleward energy transport between the tropical ocean and atmosphere. J Atmos Sci 58(8):943–948
Held IM, Suarez MJ (1974) Simple albedo feedback models of ice-caps. Tellus 26(6):613–629
Hibler WD (1979) Dynamic thermodynamic sea ice model. J Phys Oceanogr 9(4):815–846
Hoffman PF, Kaufman AJ, Halverson GP, Schrag DP (1998) A Neoproterozoic snowball earth. Science 281(5381):1342–1346
Hoffman PF, Crowley JW, Johnston DT, Jones DS, Schrag DP (2008) Snowball prevention questioned. Nature 456(7224)
Hyde WT, Crowley TJ, Baum SK, Peltier WR (2000) Neoproterozoic 'snowball Earth' simulations with a coupled climate/ice-sheet model. Nature 405(6785):425–429
Jenkins GS, Frakes LA (1998) GCM sensitivity test using increased rotation rate, reduced solar forcing and orography to examine low latitude glaciation in the Neoproterozoic. Geophys Res Lett 25(18):3525–3528
Jungclaus JH, Keenlyside N, Botzet M, Haak H, Luo JJ, Latif M, Marotzke J, Mikolajewicz U, Roeckner E (2006) Ocean circulation and tropical variability in the coupled model ECHAM5/MPI-OM. J Clim 19(16):3952–3972
Kirschvink JL (1992) The Proterozoic biosphere. In: Late Proterozoic low-latitude global glaciation: The snowball Earth. Cambridge University Press, New York, pp 51–52
Landerer FW, Jungclaus JH, Marotzke J (2007) Regional dynamic and steric sea level change in response to the IPCC-A1B scenario. J Phys Oceanogr 37(2):296–312
Le Hir G, Ramstein G, Donnadieu Y, Pierrehumbert RT (2007) Investigating plausible mechanisms to trigger a deglaciation from a hard snowball Earth. Comptes Rendus Geoscience 339(3–4):274–287
Lewis JP, Weaver AJ, Johnston ST, Eby M (2003) Neoproterozoic "snowball Earth": dynamic sea ice over a quiescent ocean. Paleoceanography 18(4):1092
Lewis JP, Weaver AJ, Eby M (2007) Snowball versus slushball Earth: dynamic versus nondynamic sea ice? J Geophys Res Oceans 112(C11):C11014
Marotzke J, Botzet M (2007) Present-day and ice-covered equilibrium states in a comprehensive climate model. Geophys Res Lett 34(16). doi:10.1029/2006GL028880
Marsland SJ, Haak H, Jungclaus JH, Latif M, Roske F (2003) The Max-Planck-Institute global ocean/sea ice model with orthogonal curvilinear coordinates. Ocean Modell 5(2):91–127
Mlawer EJ, Taubman SJ, Brown PD, Iacono MJ, Clough SA (1997) Radiative transfer for inhomogeneous atmospheres: RRTM, a validated correlated-k model for the longwave. J Geophys Res Atmos 102(D14):16663–16682
North GR (1975) Analytical solution to a simple climate model with diffusive heat transport. J Atmos Sci 32(7):1301–1307
Peltier WR, Liu YG (2008) Carbon cycling and snowball Earth Reply. Nature 456(7224)
Peltier WR, Tarasov L, Vettoretti G, Solheim LP (2004) Climate dynamics in deep time: modeling the "Snowball bifurcation" and assessing the plausibility of its occurrence. Extreme Proterozoic Geology, Geochemistry And Climate 146:107–124
Peltier WR, Liu YG, Crowley JW (2007) Snowball Earth prevention by dissolved organic carbon remineralization. Nature 450(7171):813–U1
Pierrehumbert RT (2002) The hydrologic cycle in deep-time climate problems. Nature 419(6903):191–198
Pollard D, Kasting JF (2005) Snowball Earth: A thin-ice solution with flowing sea glaciers. J Geophys Res Oceans 110(C7):C07010
Poulsen CJ (2003) Absence of a runaway ice-albedo feedback in the Neoproterozoic. Geology 31(6):473–476
Poulsen CJ, Jacob RL (2004) Factors that inhibit snowball Earth simulation. Paleoceanography 19(4):PA4021
Poulsen CJ, Pierrehumbert RT, Jacob RL (2001) Impact of ocean dynamics on the simulation of the Neoproterozoic "snowball Earth". Geophys Res Lett 28(8):1575–1578
Raval A, Ramanathan V (1989) Observational determination of the greenhouse effect. Nature 342(6251):758–761
Roeckner E, Baeuml G, Bonaventura L, Brokop R, Esch M, Giorgetta M, Hagemann S, Kirchner I, Kornblueh L, Manzini E, Rhodin A, Schlese U, Schulzweida U, Tompkins A (2003) The atmospheric general circulation model ECHAM5, part I: Model description. Tech. rep., Max Planck Institute for Meteorology, Hamburg, Germany
Roeckner E, Brokopf R, Esch M, Giorgetta M, Hagemann S, Kornblueh L, Manzini E, Schlese U, Schulzweida U (2006) Sensitivity of simulated climate to horizontal and vertical resolution in the ECHAM5 atmosphere model. J Clim 19(16):3771–3791
Romanova V, Lohmann G, Grosfeld K (2006) Effect of land albedo, CO_2, orography, and oceanic heat transport on extreme climates. Clim The Past 2(1):31–42
Rose BEJ, Marshall J (2009) Ocean heat transport, sea ice, and multiple climate states: insights from energy balance models. J Atmos Sci (in press)

Rothman DH, Hayes JM, Summons RE (2003) Dynamics of the Neoproterozoic carbon cycle. Proc Natl Acad Sci USA 100(14):8124–8129

Sellers WD (1969) A global climate model based on the energy balance of the Earth–atmosphere system. J Appl Meteorol 8:392–400

Semtner AJ (1976) Model for thermodynamic growth of sea ice in numerical investigations of climate. J Phys Oceanogr 6(3):379–389

Stone PH, Yao MS (2004) The ice-covered Earth instability in a model of intermediate complexity. Clim Dyn 22(8):815–822

Valcke S, Caubel A, Declat D, Terray L (2003) OASIS Ocean Atmosphere Sea Ice Soil users's guide. Tech. rep., CERFACS Tech. Rep. TR/CMGC/03/69, Toulouse, France, 85 pp

Walsh KJ, Sellers WD (1993) Response of a global climate model to a 30 percent reduction of the solar constant. Glob Planet Change 8(4):219–230

Washington WM, Parkinson CL (2005) An introduction to three-dimensional climate modeling, 2nd edn. University Science Books

Wild M, Roeckner E (2006) Radiative fluxes in the ECHAM5 general circulation model. J Clim 19(16):3792–3809

Wolff JO, Maier-Reimer E, Legutke S (1997) The Hamburg Ocean primitive equation model HOPE. Tech. Rep. 13. Tech. rep., German Climate Computer Center (DKRZ), Hamburg, Germany